Mapping Manufacturing Data for Stress Analysis of Automated Fiber Placement Structures

August T. Noevere[1] and Craig S. Collier[2]
Collier Research Corporation, Newport News, Virginia, 23662

The design of composite parts made with automated fiber placement technology has become an increasingly important challenge to address as this manufacturing concept matures. While automated fiber placement has many benefits, it also presents a new set of constraints that must be considered upstream during the laminate design process. Thus, a paradigm shift to design for manufacturing must be achieved to produce lightweight laminates that satisfy stress criteria while minimizing or mitigating defects. A tight coupling between stress/design and manufacturing disciplines must be achieved to understand how laminate design choices will impact the occurrence of defects, and to allow rapid iteration to alleviate the defects. Development of this coupling is the focus of this paper. In particular, a mapping process was created to translate manufacturing data from CGTech's path programming software VCP to HyperSizer, a laminate analysis and optimization tool. The tool focuses on mapping as-manufactured fiber directions and tow overlaps and gaps to the structural analysis mesh in HyperSizer so that these manufacturing features can be incorporated in stress analysis. For each of the mapping processes developed, a thorough verification is also presented to demonstrate the mapping methodology and implementation.

Nomenclature

A	=	Area of FEM element
D_{tol}	=	Tolerance for distance of projection onto FEM
D_{proj}	=	Vector tangent to tow path
$\vec{e}_m$	=	Element material axis
$\vec{f}$	=	Vector tangent to tow path
L	=	Length of lap/gap feature
$l_{s,i}$	=	Edge length of tessellation triangle on side *s* of lap/gap feature
W	=	Width of lap/gap feature
w	=	Width of tow
x	=	Coordinate of location on plane
y	=	Coordinate of location on plane
ξ	=	Area coordinate

Acronyms

AFP	Automated Fiber Placement
CAD	Computer Aided Drafting
CCT	Complex Contour Tool
CLT	Classical Lamination Theory
FEM	Finite Element Model
MS	Margins of Safety
VCP	Vericut Composite Programming

[1] Aerospace Research Engineer, Collier Research Corporation, Member AIAA
[2] President, Collier Research Corporation, Associate Member AIAA

I. Introduction

IMPROVEMENTS to Automated Fiber Placement (AFP) machines and processes in recent years has led to manufacturing capability that exceeds capability to analyze and design AFP structures. The challenges of analyzing and designing AFP structures comes from both material steering as well as features unique to the AFP manufacturing approach. The slit tape used in AFP manufacturing is narrow enough to be steered as tows are being laid down on the tool surface. This makes it possible for fiber directions in a single ply to vary significantly over the area of the part, due to either intentional steering by the designer or steering that is necessary on parts with significant curvature. It is advantageous to steer fibers in a ply to achieve better performance in a structure. However, the limits of fiber steering are a function of material and machine capabilities as well as curvature of the part. Thus, it is not always possible to select any fiber path that seems appropriate given the structural loads or stiffness requirements, and a compromise must be achieved between these requirements and manufacturing requirements.

There have been many recent efforts to perform structural optimization with AFP-manufactured structures. Approaches by Stodieck**1** and Stanford**2** use tow steering to tailor aeroelastic behavior of wings to improve flutter and divergence behavior. Both consider allowing fiber directions to vary continuously over a wing skin to provide precise control on the overall wing stiffness. At a component level, Groh**3** optimized steered tows between stiffeners in a panel to improve skin strength and buckling. A similar steering approach was applied to a subscale cylinder, representative of a composite fuselage, in the work by Wu**4**.

The feature that the above references have in common is that they allow for tow steering to generate significant fiber angle deviations within a single ply. This is the essence of a more free-form tow steering optimization; allowing the fibers to align with the dominant load direction. However, such structures can be difficult to certify due to the significant deviation from traditional 0°, 45°, 90° fiber orientations. Most laminate strength allowables used for certification of composite structures are based on these traditional orientations and incorporating non-traditional orientations cause great increases in the size of coupon test matrices.

The current work addresses the challenge of optimizing laminates for AFP manufacturing while staying as close as possible to traditional ply orientations. To accomplish this, there must be a closed loop between the tools that determine required laminate thickness and fiber orientation and the tools used to determine if fiber paths are within manufacturing limits. In the current work, this closed loop is achieved between HyperSizer5 and Vericut Composite Programming6 (VCP) software.

In addition to fiber orientation, consideration of fiber path convergence and divergence is necessary to avoid buildup of excessive tow overlaps (laps) and gaps. If two adjacent courses (passes of the machine head) can be laid down in parallel, no laps or gaps will occur where these two courses touch. If the two adjacent courses converge or diverge, tows must be cut or added to accommodate the curvature of the courses while still covering the part with material. Laps and gaps occur where the tow cuts/adds of one course touch another adjacent course. Laps and gaps can cause out-of-plane waviness in a laminate because they create a non-uniform thickness distribution at the location they occur. Additionally, gaps create discontinuities in load path, and can also lead to formation of voids in the laminate. These undesirable traits must be minimized during design of the part. Ultimately, laps and gaps are caused by selected fiber directions and part curvature. Therefore, the occurrence of laps and gaps must be considered when fiber directions are being selected for strength and stiffness constraints. The location, size, and shape of laps and gaps must be relayed to laminate optimization tools to achieve this closed loop. In the work discussed in this document, lap and gap shapes calculated in VCP are mapped to the Finite Element Model (FEM) in HyperSizer to account for their impact on laminate optimization.

To achieve the transfer of fiber path information and lap/gap information described above, a data mapping interface was established between VCP and HyperSizer. The primary challenge of developing this interface was that VCP operates on a Computer Aided Drafting (CAD) representation of the part, while HyperSizer operates on a FEM representation of the part. As a result, representations of fiber paths and lap/gap geometry in VCP are continuous in nature and the equivalent representations in HyperSizer are discrete in nature. To map data between the two software packages, it is necessary to develop approaches to translate the AFP data from a continuous (CAD) to discrete representation (FEM).

A. Overview of Workflow and Data Interface

Figure 1 provides an overview of the interface process between HyperSizer and VCP. The steps of the process are described below.

1. The workflow starts with HyperSizer, which is able to determine optimum ply shapes, counts, and orientations that satisfy strength and stability analyses for a selected material and applied loads. At this point, the laminate is in a FEM-based representation.
2. To get the optimized plies into VCP, it is necessary to translate the plies to a CAD-based representation. This is currently done in CATIA7, where CAD curves are fit through the FEM grid points to create a smooth, continuous representation of the ply boundaries. Additional features are used in CATIA's Composite Workbench to generate a ply file that can be imported by VCP.
3. Once the tool geometry (CAD surface) and ply representation (boundaries and orientations) have been imported, VCP uses this information to generate tow paths that fill the ply boundaries with material. This process requires the user to define AFP process parameters related to the AFP machine and desired layup performance
4. After tow paths have been generated in VCP, data related to AFP manufacturing is mapped back to HyperSizer for inclusion in the stress analysis and optimization. This data includes as-manufactured fiber directions and lap/gap geometry. Developing the data mapping described in this step is the primary focus of the current work.

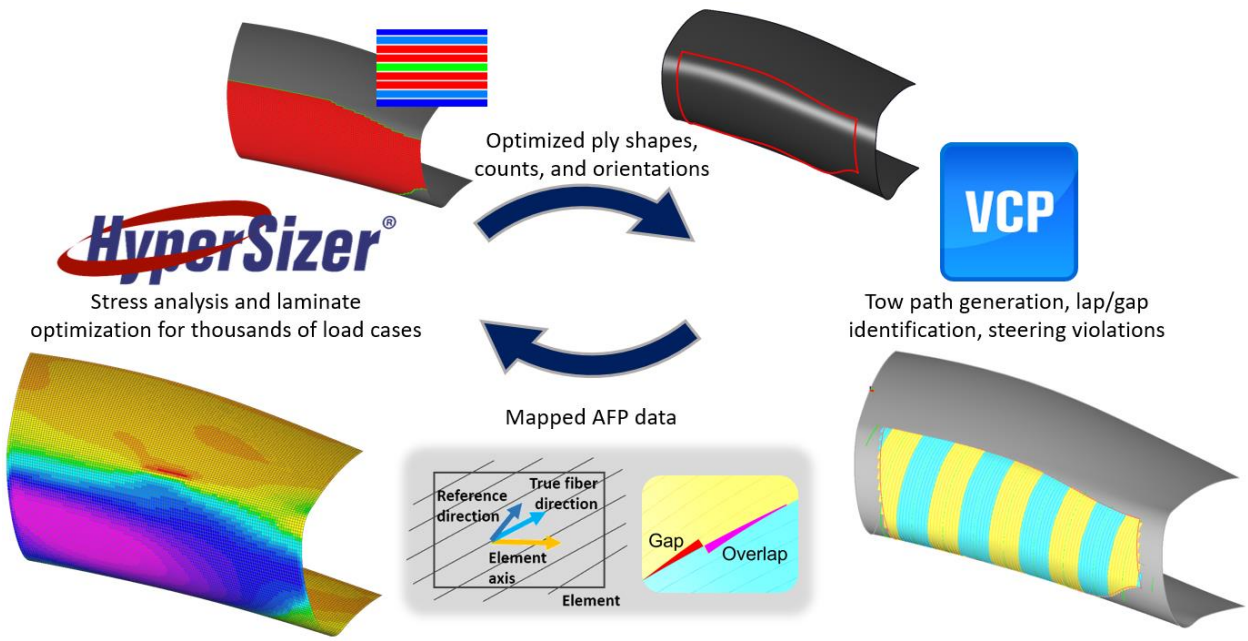

Figure 1. Overview of HyperSizer-VCP interface.

This document presents the details of the methods used to map the data described above, with the following three sections each focusing on true fiber direction mapping, lap/gap mapping, and steering violations mapping. Additionally, thorough verifications of these data mappings are presented to demonstrate that the methods are sound and were implemented correctly.

B. Test Model for Development

The test model used for development and verification of the VCP interface is the "Complex Contour Tool" (CCT), shown in Fig. 2. This tool was selected because it contains a sufficient amount of double curvature to be challenging from the perspective of AFP manufacturing. The curvature is such that constant angle or "rosette" fiber orientations are not possible over the entirety of the tool without aggressive steering of tows. A tool with such curvature requires iteration between stress analysis and AFP manufacturing planning.

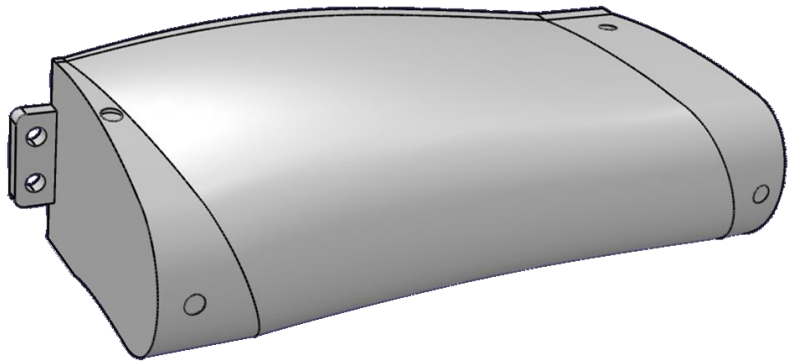

Figure 2. CAD model of CCT.

In addition to the CAD model of the CCT, a FEM model (shown in Fig. 3) was also developed because this is needed for stress analysis in HyperSizer. The FEM mesh contains 18,001 quadrilateral elements. To generate internal loads, an opening force was applied to the top and bottom of the structure, with boundary conditions that allow a free opening of the structure. This force generates bending moment in the C-shaped portion of the structure.

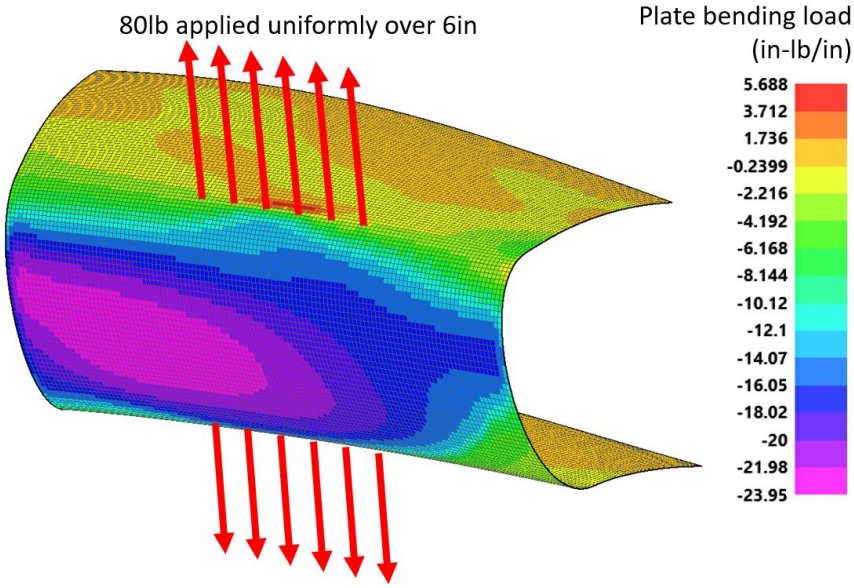

Figure 3. FEM of CCT and applied loads.

The internal bending moments were used in HyperSizer to generate an optimum laminate that supports the applied loads. HyperSizer optimized the structure using generic carbon/epoxy tap material properties, given in Table 1.

Table 1. Material properties used by HyperSizer.

Property	Unit	Value
E_1 (Stiffness, 1-dir)	Msi	20
E_2 (Stiffness, 2-dir)	Msi	1.4
G_{12} (Shear Stiffness)	Msi	0.5
ν_{12} (Poisson's Ratio)	-	0.34
$F_{u,1}$ (Ultimate Stress, 1-dir)	Ksi	100
$F_{u,2}$ (Ultimate Stress, 2-dir)	Ksi	14
$F_{su,12}$ (Ultimate Shear Stress)	Ksi	6
$e_{u,1}$ (Ultimate Strain, 1-dir)	µin/in	5000
$e_{u,2}$ (Ultimate Strain, 2-dir)	µin/in	10000
$es_{u,12}$ (Ultimate Shear Strain)	µin/in	10909.09

The material properties given above were used to generate optimized laminates for the model. With these material properties and the applied loads, HyperSizer created a laminate that has a maximum of 9 plies. The ply counts and laminates over the structure are shown in Fig. 4. Note that the optimization was required to generate a balanced and symmetric laminates, as well have at least one ply of each orientation.

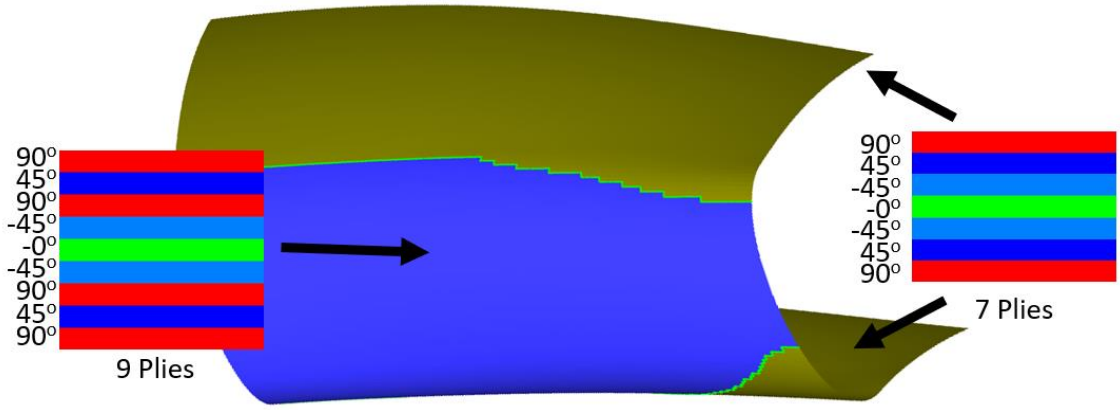

Figure 4. Optimized laminates output from HyperSizer.

The laminates from HyperSizer were transferred to VCP using the process described previously. In VCP, tow paths were generated for each ply in the laminate to match the coverage specified by the HyperSizer optimization. For this path generation, 0.5" tows were used, with 10 tows in each course. The tows were allowed to overlap by up to 0.25" (only in convergence regions where tow cuts were required) so that both laps and gaps would appear in the plies. The tows generated for plies 1-3 are shown in Fig. 5 below. The remainder of the plies are shown in Appendix A.

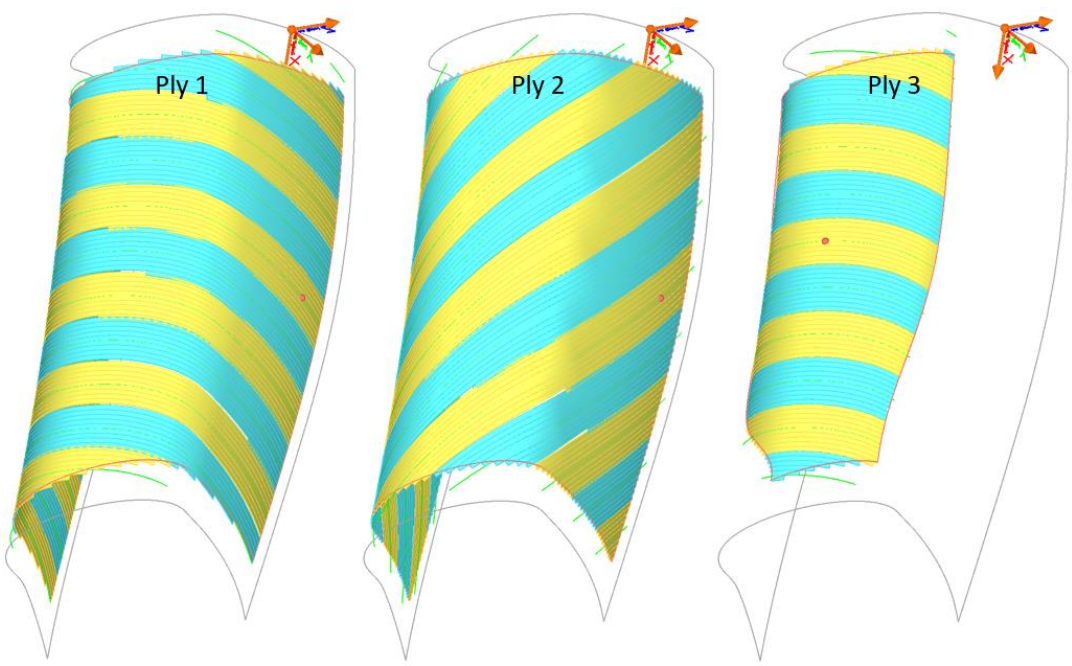

Figure 5. Tow coverage from VCP for plies 1-3.

II. Mapping True Fiber Directions

VCP is a software package used to generate tow paths on a part. The user has control over steering the tow paths and can also evaluate viability of the tow paths. These tow paths are generated on CAD surfaces representing the tool surface and each tow path itself is essentially a CAD surface. Thus, VCP has knowledge of the "true" (as-

manufactured) fiber paths over the entirety of the part, for every ply. It is this information that is extracted to be passed back to HyperSizer for inclusion in strength and stiffness analyses. Without this information, HyperSizer is only able to analyze the material based on reference material directions assumed during the creation of the FEM. The sections below describe the methodology used to map the true fiber directions from VCP to the FEM mesh in HyperSizer, as well as methods to verify this mapping.

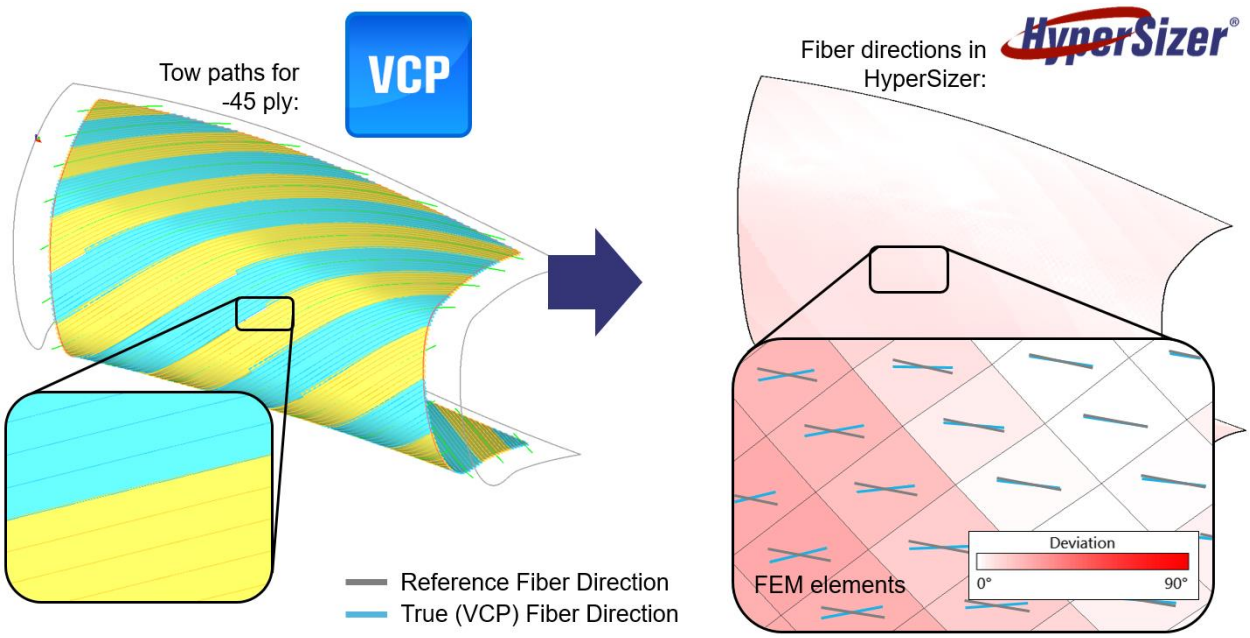

Figure 6. Concept of fiber direction import from VCP to FEM mesh in HyperSizer.

A. Mapping Methodology

The primary challenge of mapping true fiber directions from VCP to HyperSizer is that VCP represents the fiber paths as continuous CAD-based entities, whereas HyperSizer is a FEM-based tool that represents surfaces with discrete elements. The chosen approach was to extract fiber directions for each FEM element at the centroid of the element. This requires that HyperSizer pass a list of XYZ points to VCP corresponding to all of the element centroids in the part and VCP extracts the fiber directions at these locations. This process is depicted in Fig. 7 for a single ply.

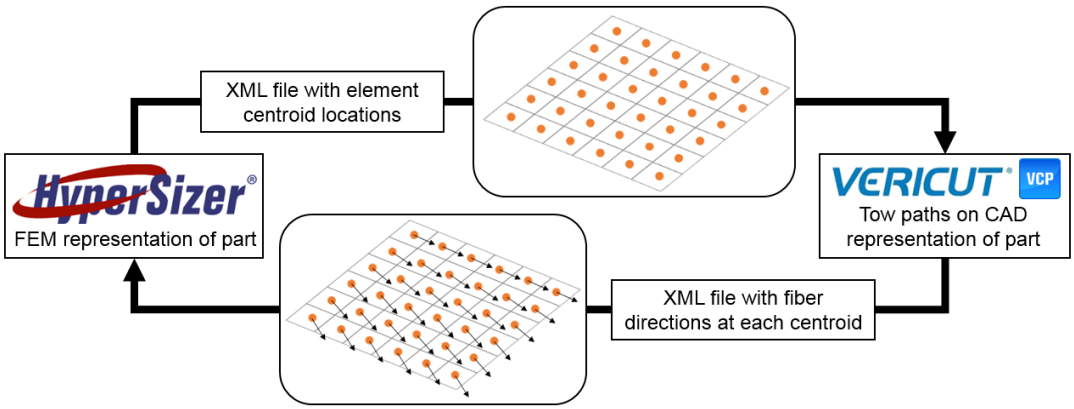

Figure 7. Mapping true fiber directions onto FEM mesh in HyperSizer.

The fiber directions from VCP are exported as unit vectors tangent to the fiber direction at the element centroid location. HyperSizer translates the fiber direction in each element from a unit vector to an angle measured from the element's material axis. This calculation is shown in Eq. 1, where $\vec{f}$ is the fiber direction unit vector (after projection into the plane of the element) and $\vec{e}_m$ is the vector of the element material axis.

$$\theta_{fiber} = \cos^{-1}\left(\frac{\vec{f} \cdot \vec{e}_m}{|\vec{f}||\vec{e}_m|}\right) \tag{1}$$

B. Verification of Mapping

The fiber angle calculation was verified with manual calculations for a subset of the elements. The process performed that is performed internally in HyperSizer to determine the angle between the true fiber direction and element material axis was manually recreated in an Excel spreadsheet. This process consists of:

1. Determine vector for element normal
    a. Calculate normal of planes formed by 1-2-4 nodes and 2-3-4 nodes (for quad elements)
    b. Average above normal vectors
2. Determine vector for element material axis
    a. Calculate vector between element nodes 1 and 2
    b. Rotate vector about element normal by value specified for element material orientation
3. Determine reference material direction for element, for current ply
    a. Rotate element material axis by the value of the ply orientation (0, 45, -45, or 90)
4. Determine deviation angle between reference material direction and fiber direction vector from VCP
    a. Project both into the plane defined by the element normal
    b. Calculate the angle between the vectors
5. Compare calculated deviation angle to result reported by HyperSizer

This process was performed with 25 data points, consisting of a random selection of element and ply combinations. As such, a variety of elements over the area of the part were examined, and each of the 9 plies were also checked (representing 0, 45, -45, 90 orientations.) Because of this comprehensive representation of the laminate data, and the small amount of error encountered, these 25 data points were deemed sufficient to verify the mapping. A summary of the error found is reported in Table 2 below.

Table 2. Error (degrees) summary for mapped VCP fiber directions

	All Data	0 plies	45 plies	-45 plies	90 plies
Min	-0.00498	-0.00414	-0.00367	-0.00084	-0.00498
Max	0.06163	0.06163	0.00554	0.00136	0.01456
Mean	0.00388	0.02070	-0.00007	-0.00006	0.00136
Std Dev	0.01333	0.02940	0.00294	0.00123	0.00511

As Table 2 shows, the documented error in the process is very low and could be attributed to compounded numerical rounding issues. Error from such a source can become slightly noticeable when very small numbers are used in trigonometric operations, as is the case with these calculations. Another potential source of error is that the method described above to manually calculate the material directions could potentially be slightly different than the method implemented in HyperSizer's element processing code (directly copying the HyperSizer code would have invalidated the verification). Because quadrilateral FEM elements are bilinear surfaces, all four nodes are not in the same plane. As a result, numerous vector transformations must be performed to calculate fiber orientations. Even changing the order of the transformations can impact the calculated fiber deviation angle.

III. Mapping Tow Overlaps and Gaps

The tow overlaps (laps) and gaps that occur on most AFP structures can result in non-uniform ply and laminate thickness. Laps and gaps usually occur in pairs at locations where tows of one course are cut at the intersection with another course. Designers can control whether more laps or more gaps occur, to the extremes of having either all laps (no gaps) or all gaps (no laps). Figure 8 shows the occurrence of a gap and lap between two adjacent courses.

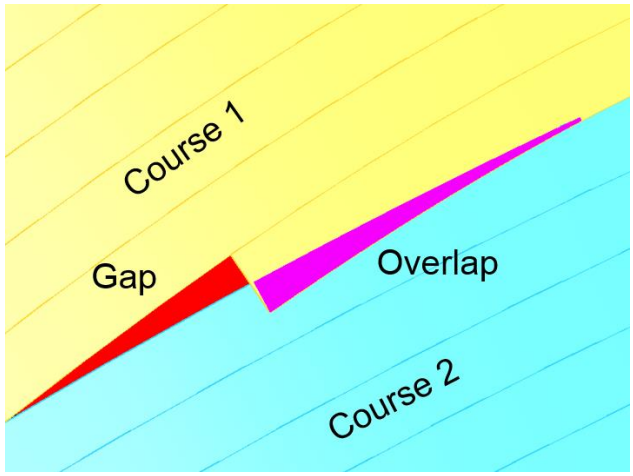

Figure 8. Gap (red) and overlap (violet).

Tow laps cause ply thickness to be doubled at the lap location. Conversely, gaps form a discontinuity in the ply. Both of these features can have an impact on the integrity of the part and therefore must be considered during stress analysis while sizing the part. Thus, it is necessary to map the geometry of the laps and gaps that VCP identifies to the FEM mesh in HyperSizer that forms the basis of the stress analysis. The sections below describe the method used to map the CAD representations of the laps and gaps to the FEM mesh in HyperSizer, as well as a verification of that method.

A. Mapping Methodology

Mapping the lap and gap features from VCP to HyperSizer requires translating the physical geometry of the laps and gaps into per-element quantities that can be associated with the FEM mesh. Figure 9 provides an overview of the process.

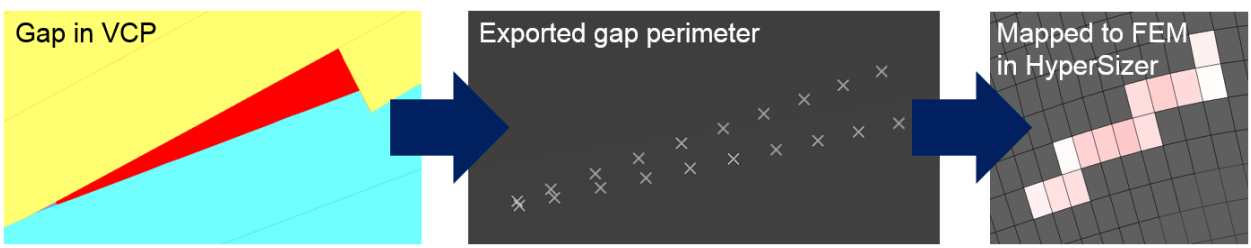

Figure 9. Lap and gap mapping approach.

The mapping requires discretizing the lap and gap features and determining which FEM elements they map to based on proximity. Discretization of the lap and gap features is done by tessellating their geometry. The triangles generated from the tessellation are used to determine which FEM elements the lap or gap lies on, so that the properties of the lap or gap (area, length, and width) can be mapped to these elements. This process is depicted in Fig. 10.

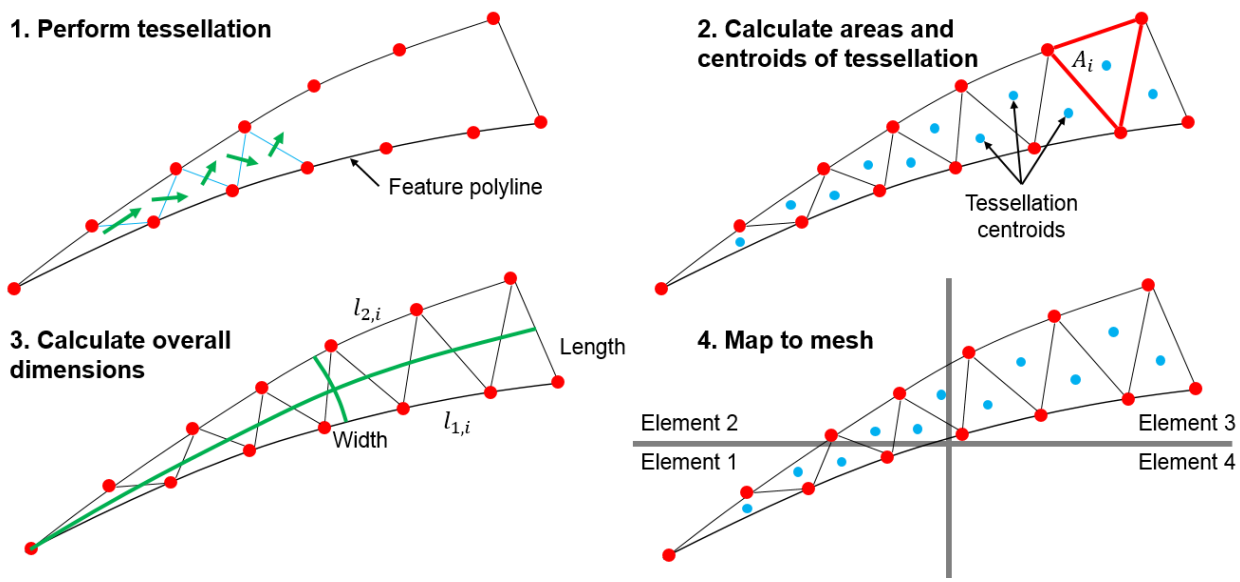

Figure 10. Tessellation and mapping of lap and gap features to FEM mesh.

The first step is tessellating the lap or gap geometry from VCP. The geometry is represented with a polyline of the lap or gap perimeter, which contains evenly spaced points along the perimeter. This is the same data that VCP outputs for laser projection systems to aid with visual inspection during manufacturing. The format of this data output also makes it useful for tessellation.

Due to the even spacing of the polyline points, tessellation of the feature can be easily performed by drawing triangle edges back and forth between the lap or gap sides going down the length of the feature. The tessellation algorithm relies on this geometry representation being consistent.

Once the tessellation triangles have been formed, the next step is to determine their centroid locations as well as area. These individual areas are summed up to determine the total area of the feature. The centroid locations are used to determine the element coverage of the lap or gap in scenarios where it may cover multiple FEM elements.

Next, the overall dimensions of the lap or gap are calculated. Because the lap or gap can potentially cover significant distance over a curved surface, the lap or gap length cannot be calculated directly from the Euclidean distance between the two ends of the feature. Instead, it is necessary to calculate length along the curvature of the part. This is simple to determine by summing the length of the tessellation triangle edges on either side of the feature ($l_{1,i}$ and $l_{2,i}$) and finding the average of the two sides, as shown in Eq. 3. Average width of the feature is then calculated by dividing the total feature area from Eq. 2 by the length, as shown in Eq. 4.

$$A = \sum_{i=0}^{n} A_i \tag{2}$$

$$L = \frac{1}{2}\left(\sum_{i=1}^{n_1} l_{1,i} + \sum_{i=1}^{n_2} l_{2,i}\right) \tag{3}$$

$$W = A/L \tag{4}$$

The final step is to map all of the tessellation triangles to the FEM mesh. This is done with a projection and proximity-based approach, depicted in Fig. 11. The process loops through each tessellation triangle and finds an element which the triangle centroid can project into and which is within a specified distance tolerance (typically 10% of average element size) from the triangle centroid.

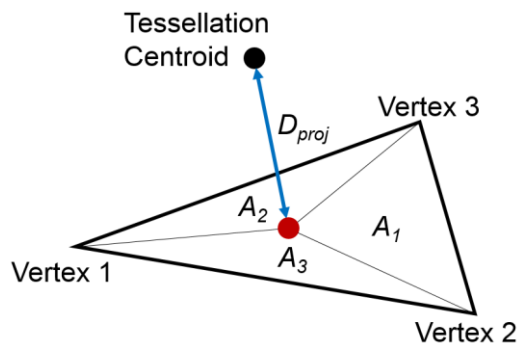

Figure 11. Method for determining elements for lap or gap mapping.

To determine if the centroid projects into the element, the centroid is first projected into the plane of the element formed by the three nodes of the elements (thus, only triangular elements can be used; quadrilateral elements are split in half from node 1 to node 3). Next, the area coordinates of the projected tessellation centroid are calculated with respect to the three nodes of the element, as shown in Eq. 5 through 7, where A is the total area of the element and x,y are coordinates in the plane of the element measured from an arbitrary origin.

$$\xi_1 = \frac{1}{2A}\left((x_2y_3 - x_3y_2) + (y_2 - y_3)x + (x_3 - x_2)y\right) \tag{5}$$

$$\xi_2 = \frac{1}{2A}\left((x_3y_1 - x_1y_3) + (y_3 - y_1)x + (x_1 - x_3)y\right) \tag{6}$$

$$\xi_3 = \frac{1}{2A}\left((x_1y_2 - x_2y_1) + (y_1 - y_2)x + (x_2 - x_1)y\right) \tag{7}$$

If the area coordinates are all positive, then the tessellation centroid was successfully projected into the element. Finally, the distance between the tessellation centroid and the projection into the plane is calculated to ensure that $D_{proj}<D_{tol}$. This is necessary because it is possible for the tessellation centroid to project into multiple elements if the surface is highly curved. Applying a tolerance to the projection distance ensures that the lap or gap is only mapped to elements in its immediate vicinity.

The program implementation of the tessellation and mapping process described above is depicted in the diagrams in Appendix B.

B. Verification of Mapping

Verification for this mapping is necessary to ensure that lap or gap geometry was correctly mapped to the FEM mesh. The first step of the verification is to demonstrate that the tessellation of the lap/gap features from VCP is performed correctly. Next, the lap/gap geometry (length, width, area) calculations from the tessellated representation are compared to the original CAD representation from VCP. Finally, the mapping of lap/gap geometry to the FEM mesh is verified by checking that the FEM elements were assigned the correct geometry values. These three steps are shown in the following sections.

1. Tessellation of Lap/Gap Features

To verify that the tessellation of the features is performed correctly, it is first necessary to check that the feature perimeter points described in the previous section line up with the true lap/gap geometry found in VCP. Figure 12 below shows an example of this alignment. Additionally, this alignment was checked for over 100 lap/gap features and no issues were found.

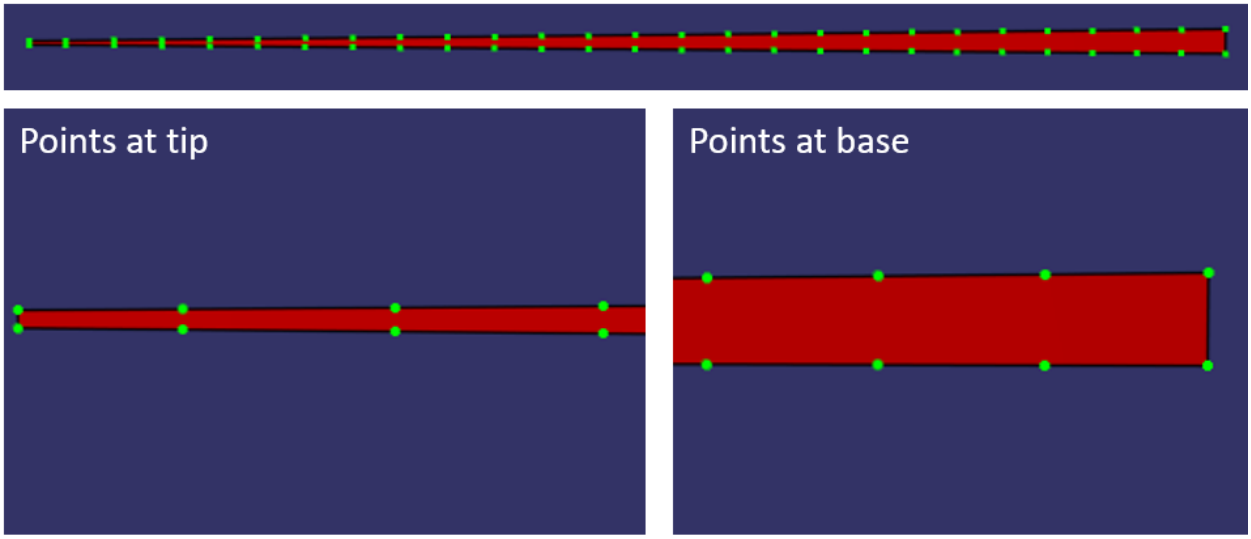

Figure 12. Alignment of perimeter points with original feature geometry from VCP.

To verify the tessellation itself, the tessellated features are compared to the original lap/gap CAD geometry from VCP. This comparison is shown in Fig. 13 below. This tessellation alignment was checked for over 100 lap/gap features and no issues were found.

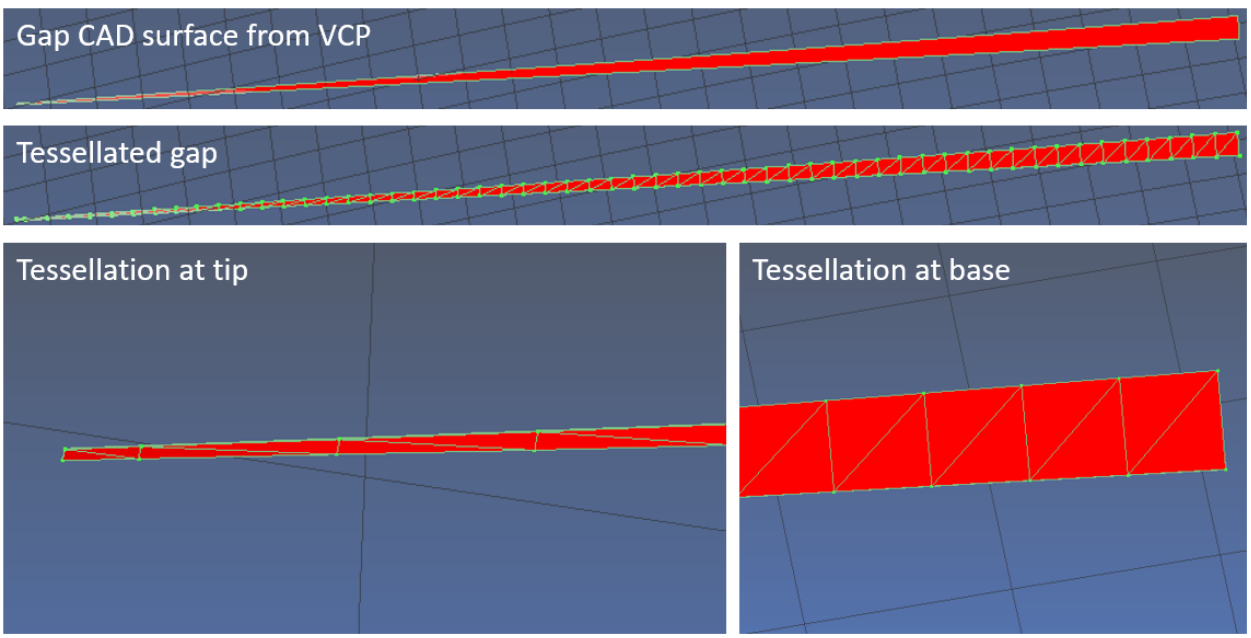

Figure 13. Verification of tessellation.

2. Calculating Lap/Gap Feature Geometry from Tessellation

The calculation of length, width, and area of the lap/gap features is performed based on the tessellated feature geometry, not the original CAD geometry. For this reason, it is necessary to verify that the calculated feature geometry matches the feature geometry measured in CAD software. This was done for 25 laps and 25 gaps (randomly selected from all 9 plies). Figure 14 shows the geometry measurements that were verified.

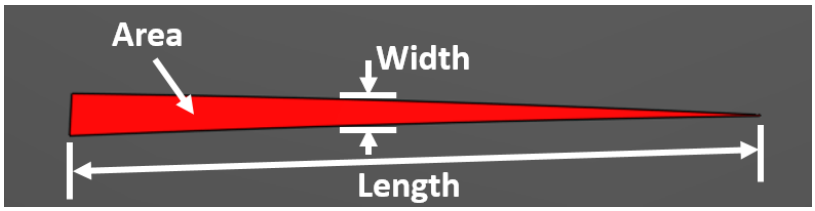

Figure 14. Lap/gap feature geometry measured for verification.

For all of the 50 features sampled, geometry measurement error was found to be very low. A summary of the measurement error percentages is provided in Table 3 below.

Table 3. Statistics of lap/gap geometry measurement error (%).

		Length	Width	Area
Laps	Min	-0.014	-1.563	-0.196
	Max	0.462	0.000	0.000
	Mean	0.015	-0.063	-0.010
	Std Dev	0.093	0.313	0.040
Gaps	Min	-0.027	-0.461	0.000
	Max	0.009	0.943	0.035
	Mean	-0.002	0.019	0.001
	Std Dev	0.008	0.213	0.007

3. Mapping Lap/Gap Geometry to FEM Mesh

The final part of the process to verify is mapping from the lap/gap tessellation to the FEM mesh. This requires demonstrating that the correct FEM elements were assigned the correct feature geometry values, according to where the centroid of each tessellation triangle lies. This verification is mostly visual, and results in either a pass or fail for the mapping. An example of the verification is shown for a gap from ply 1 in Fig. 15 below. Elements which have mapped data corresponding to the feature geometry are colored yellow. The green points indicate the centroids of the tessellation triangles, which were used to perform the mapping to the FEM mesh. Figure 15 clearly shows that the only elements receiving mapped data are those covered by lap/gap tessellation centroids, indicating a successful mapping. The mapping to the mesh was found to be very accurate; the mapping was performed 100% correctly for all 100+ features examined in the CCT laminate.

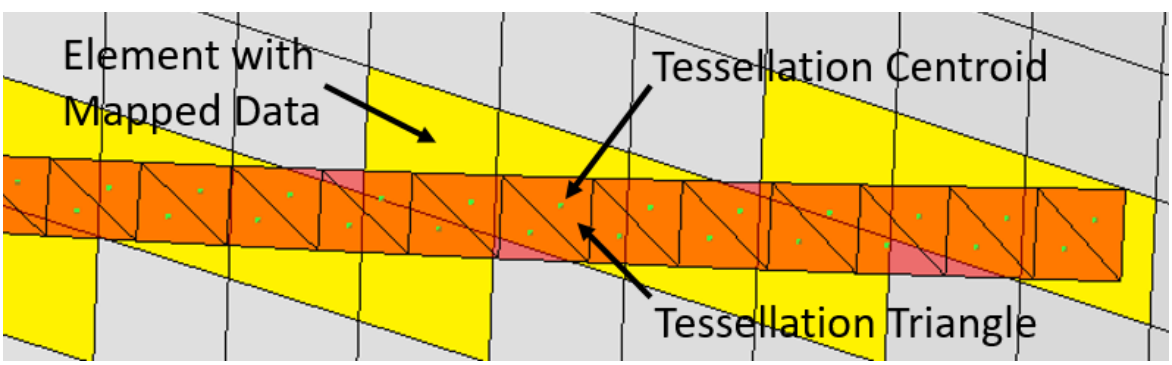

Figure 15. Verification of mapping to FEM mesh.

Mapping of laps and gaps can also be verified from a more high-level view to determine if any of the features were completely missed in the mapping. Figure 16 shows an example of this high-level verification. Note that the cyan line indicates the boundary of the ply (which coincides with the boundary of the FEM in this case).

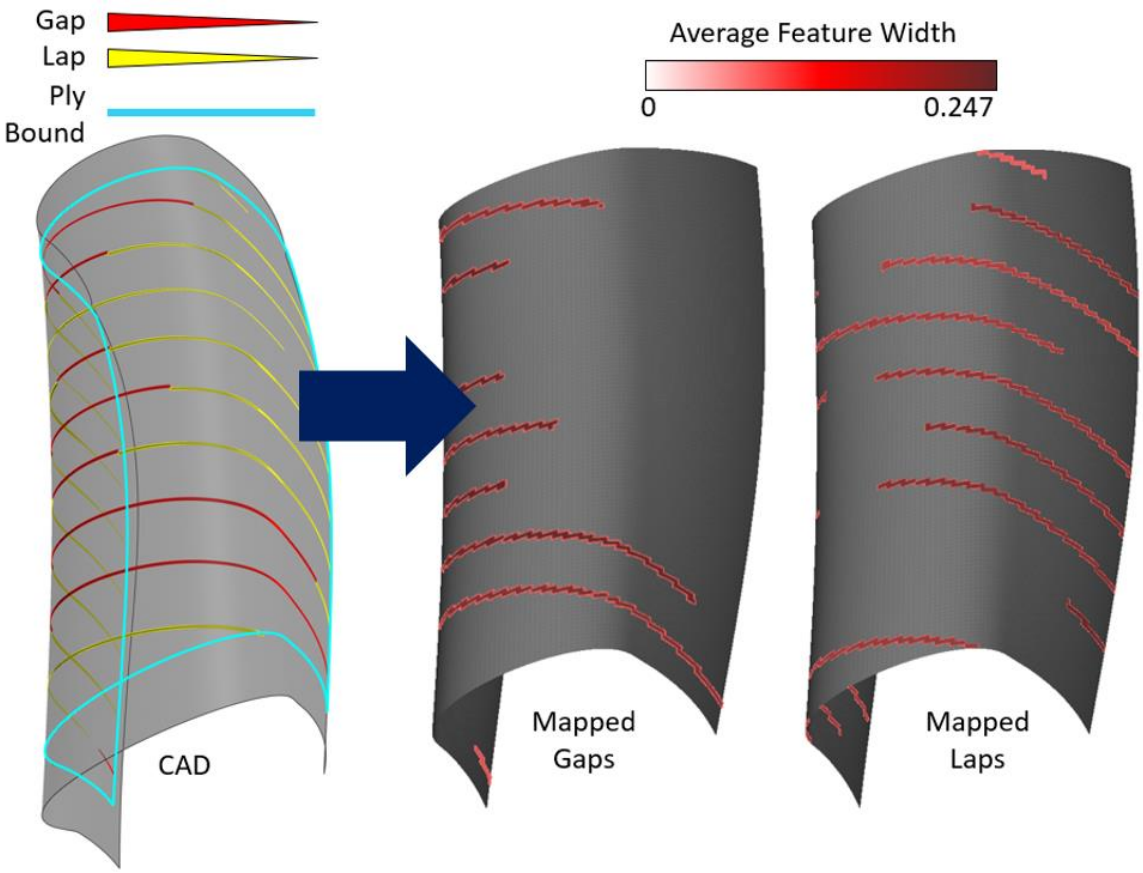

Figure 16. High-level verification of lap/gap mapping for ply 1.

IV. Stress Analysis and Re-Design Incorporating AFP Data

With the capabilities described above to map data from VCP to HyperSizer, stress analysis was performed with the as-manufactured fiber directions and gaps. Negative strength margins were encountered from this analysis due to fiber deviations and missing material at gap locations. Using the interface between VCP and HyperSizer, the laminate design was modified to resolve these issues. This was made possible by the rapid exchange of AFP manufacturing data and strength analysis data.

A. Stress Analysis with True Fiber Directions

The true fiber directions mapped to the FEM were used to run an updated stress analysis on the laminate. In the optimization that produced the laminates, a rosette direction was assumed for the plies. This rosette direction aligns with the primary axis of curvature in the CCT model. The 0°, +45°, -45°, 90° plies were assumed to be oriented relative to this rosette direction. However, the true as-manufactured fiber directions vary from these assumed orientations due to the tool curvature. This deviation is enough to impact the strength margins of the laminate.

The stress analysis approach used for the CCT is a ply-based analysis using Classical Lamination Theory (CLT). For each element, the specified laminate design is used to build an ABD stiffness matrix for the laminate. This stiffness matrix includes the impact of fiber angle deviation. Using the membrane and bending loads from the element, local laminate deformation is then calculated and resolved into ply strains and stresses. Strain and stress output is used to write margins for each ply, considering a variety of failure criteria. These include max strain and max stress for the 1, 2, and 12 directions, as well as several interaction criteria including Tsai-Hill, Tsai-Hahn8, Tsai-Wu**9**, and Hoffman criteria.

In the original analysis, the laminate had all positive MS which were close to zero as is expected for an optimized structure. After inclusion of the true fiber direction from AFP manufacturing, many of the margins become negative in the more highly loaded portion of the laminate. The comparison between these two margins is shown in Fig. 17 below.

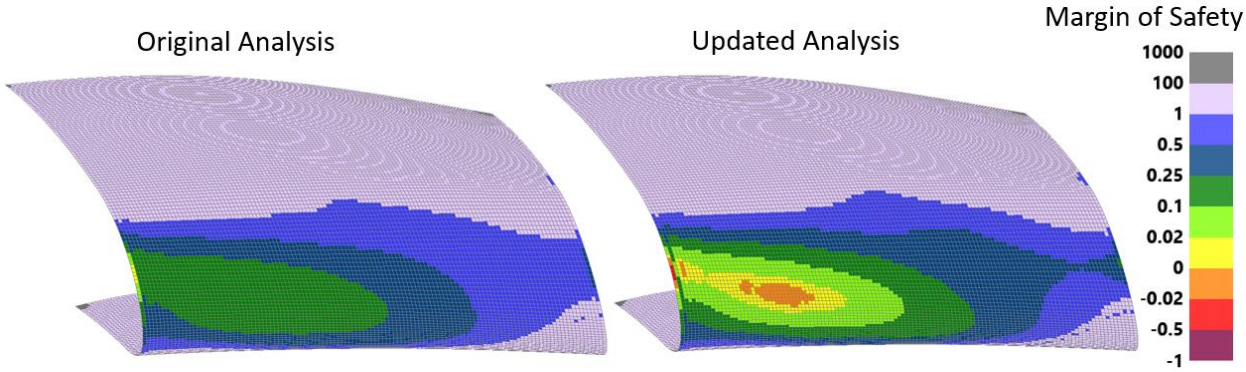

Figure 17. Updated margins from true fiber directions.

These negative margins are mostly due to fiber deviations occurring in the "C" shaped portion of the CCT. The applied opening load creates a bending moment in this region, which is reacted by 90° fibers. Thus, deviation of these 90° fibers causes strength margins to become negative in this region. Figure 18 below shows deviation of the 90° plies on the outside of the laminate, which are most critical for supporting the bending load in this region. Deviation up to 10° from the rosette direction is observed.

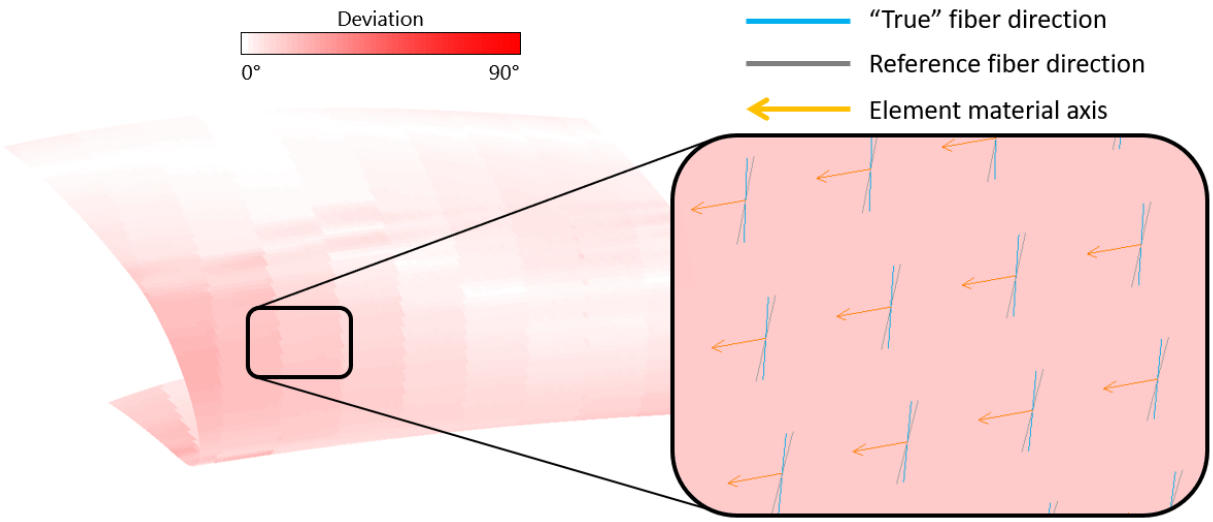

Figure 18. Fiber deviation in outer 90° ply.

Another consideration for fiber deviation is the desire to minimize relative thru-thickness deviation in the laminate from a local 0°, 45°, 90° laminate stack-up. A [0/45] laminate that is actually a [10/55] in a particular location, as manufactured by AFP, is still acceptable because locally it is still a [0/45], just rotated by 10°. However, an as-manufactured laminate of [0/55] would be unacceptable because of the 10° relative deviation between plies. These rules are usually enforced to maintain validity of laminate-based allowables used for certification, which are based on laminates with 0°, 45°, 90° orientations only.

The relative deviation for the CCT is shown in Fig. 19 below. Portions of the structure exceed the typical 2° limit and will be addressed in the laminate re-design.

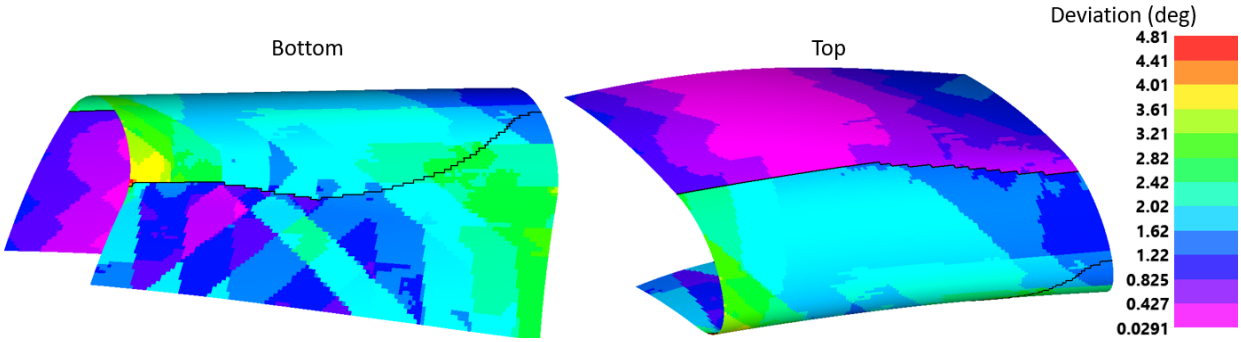

Figure 19. Relative through-thickness deviation from nominal 0º, 45º, 90º directions.

B. Stress Analysis of Gaps

Gaps are analyzed with a simple thickness scaling approach in the ply-based analysis. For elements that are covered by a gap for a particular ply, the thickness of that ply is scaled down by the amount of gap coverage. For example, an element that has 50% of its area covered by a gap in a given ply will have a 50% reduction of thickness in that ply in the CLT analysis. This is depicted in Fig. 20.

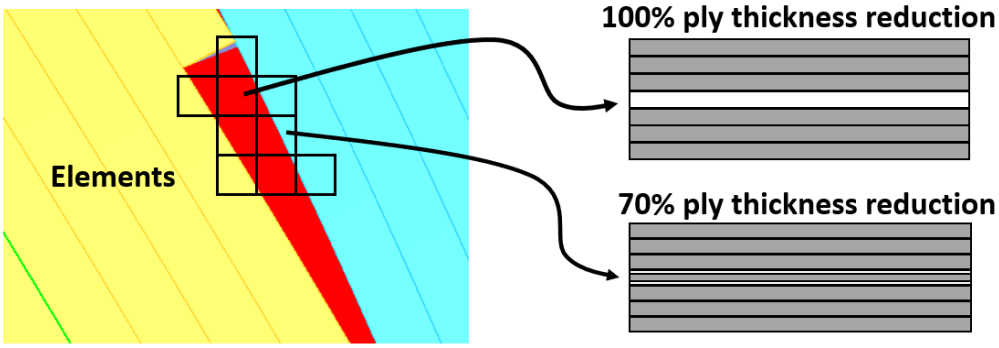

Figure 20. Thickness reduction scheme to account for gaps in CLT analysis.

Overlaps were not analyzed this way because the thickness scaling would actually increase the strength of the laminate in the location of the overlap. Because laps are often classified as a defect, this analysis was not implemented to avoid a knock-up to the laminate strength.

After mapping the gaps to FEM, they were analyzed with the approach described above. The inclusion of gaps brought the strength margins down further, as shown in Fig. 21.

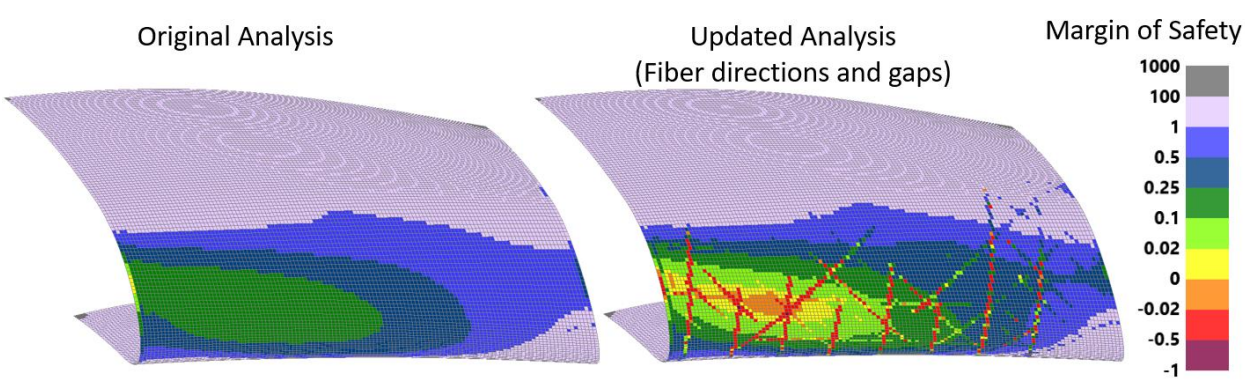

Figure 21. Margins updated with tow gap analysis.

One reason for the significant negative margins from gaps is due to the symmetry of the laminate. The exact same tow paths were used for symmetric plies. As a result, each gap lines up with at least one other gap. This is addressed in the re-design by staggering the tow locations to avoid stacking multiple gaps.

C. Tow Steering Radius Considerations

Steering of the tows is an important consideration for AFP structures due to the defects that can occur on a complex curvature surface**10**. For this structure, only natural paths were used so that significant steering was not present, mitigating the chance that defects such as tow wrinkling or puckering would occur. On a highly complex curvature surface, natural paths can cause significant fiber angle deviation. This occurred in some areas on the CCT, but was ultimately mitigated with the laminate modifications described below.

D. Design Modifications

Considering the negative strength margins and fiber deviation challenges discussed above, the laminate was modified to resolve these issues. Steps that were taken to resolve the issues and find an acceptable design:

1. Added a 0° ply at the midplane of the laminate on the "C" shaped portion of the structure. This moved the 90° plies further away from the neutral axis of the laminate, improving ability to carry bending load even with fiber deviation. This increased the overall weight from 5.88lb to 6.13lb.
2. Staggered gaps so that fewer gaps from multiple plies coincide.
3. Rotated the smaller 90° plies to reduce the amount of relative through-thickness deviation over the structure.

These changes produce the margins shown in Fig. 22 below. The "C" shaped portion of the structure has the lowest margins, but all margins are positive after the design changes described above. The gaps are visible as strips of lower margins.

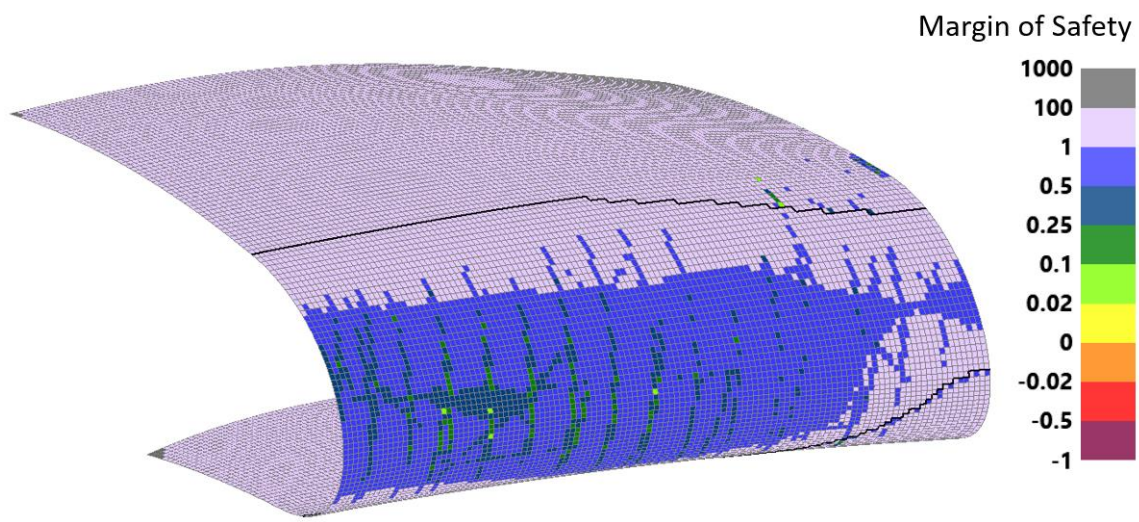

Figure 22. Margins after design modifications.

Fiber angle deviation was tracked during the laminate re-design and was minimized as much as possible. The maximum deviation was reduced from 4.81° to 4.03° and the surface area of laminate with deviation greater than 2° was reduced from 15.4% to 6.3%. The deviation from the re-designed laminate is shown in Fig. 23.

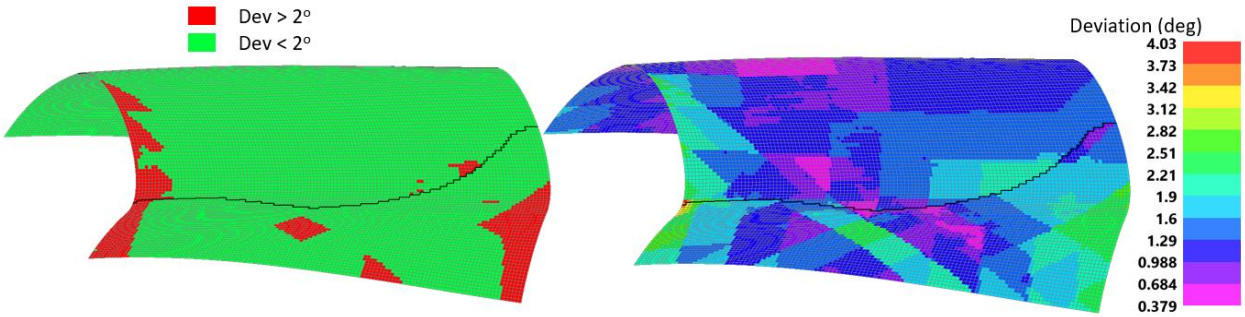

Figure 23. Relative through-thickness deviation from nominal 0°, 45°, 90° directions after modification.

V. Conclusion

The presented methodology has been demonstrated to successfully map manufacturing data from VCP to HyperSizer with very little error in the mapping processes. This includes the mapping of as-manufacturing fiber directions (at each element) and mapping of lap and gap geometry (length, width, and area). This mapping allows for rapid iteration between stress analysis and AFP manufacturing planning. This design environment facilitates weight optimization of AFP laminates through modification of tow paths, ply counts, ply boundaries, and ply orientations. The design environment was demonstrated on a complex curvature tool by finding a laminate design with positive strength margins that met manufacturing AFP requirements.

Appendix

A. VCP Tow Paths Used in Verification

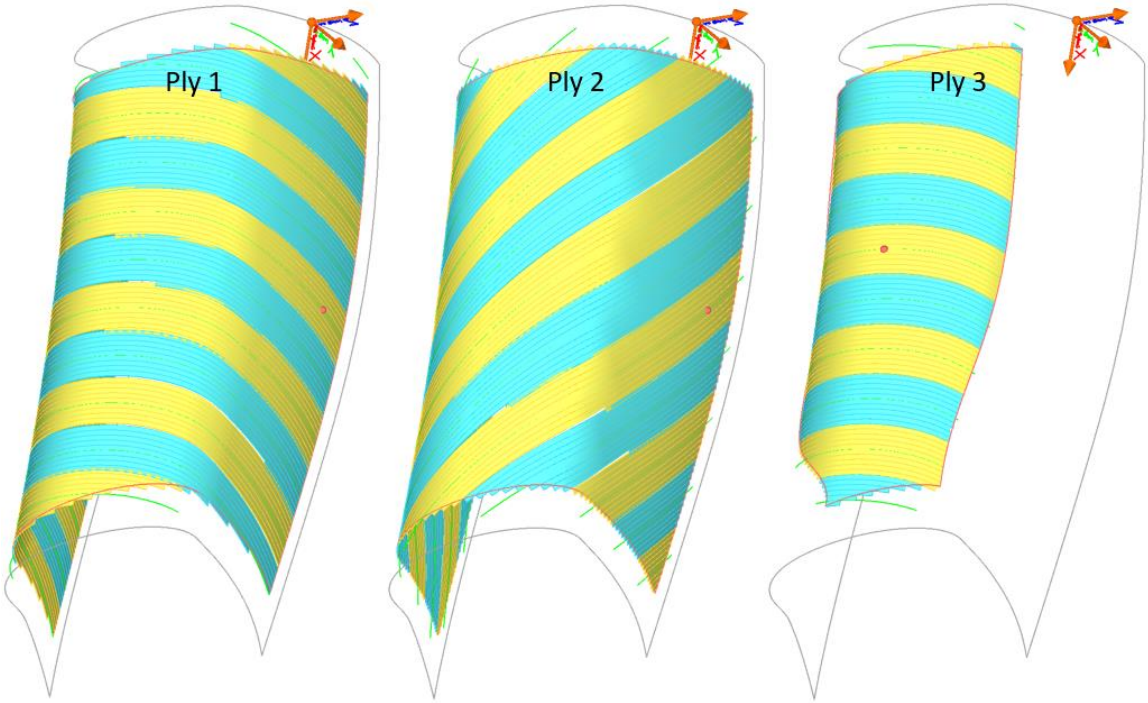

Figure 24. VCP plies 1-3.

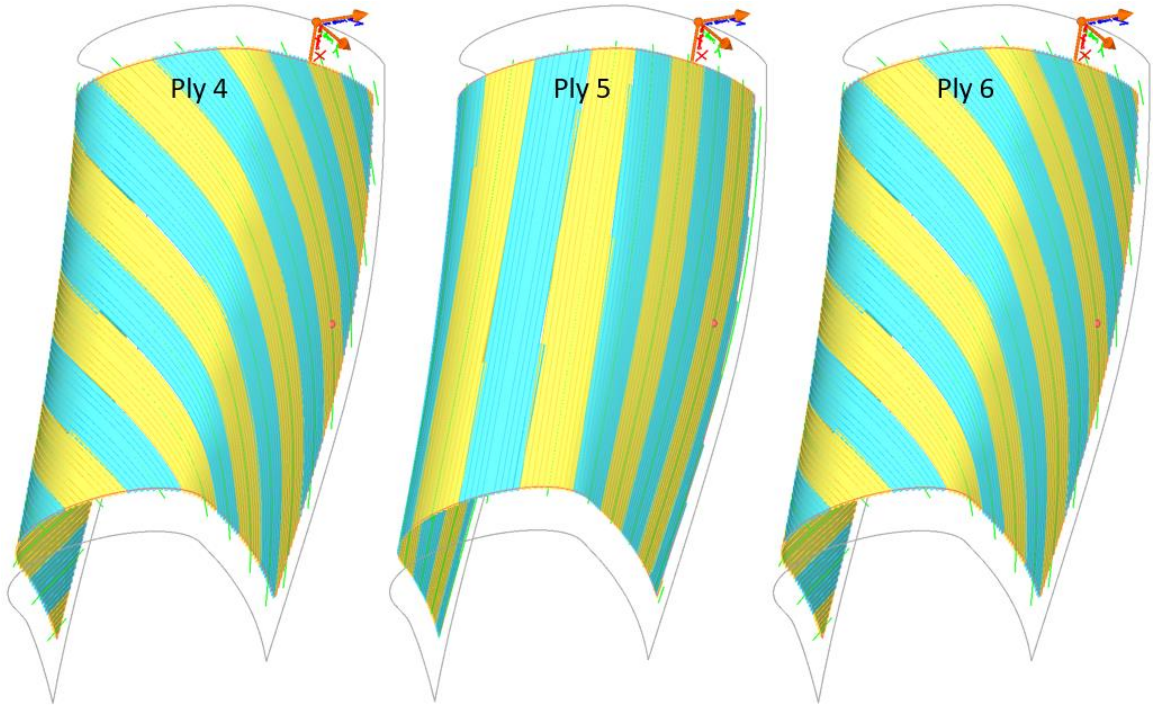

Figure 25. VCP plies 4-6.

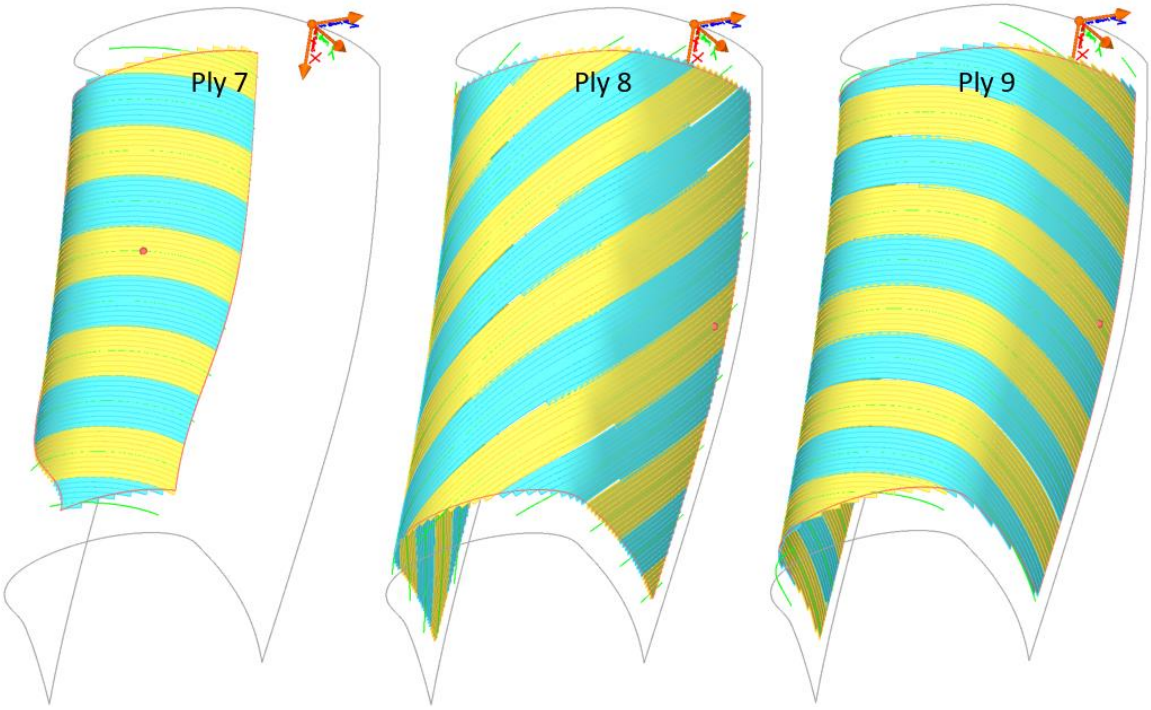

Figure 26. VCP plies 7-9.

B. Program Flow Diagrams

This appendix contains diagrams that depict how the data mapping processes were implemented in HyperSizer.

1. *Mapping Fiber Directions*

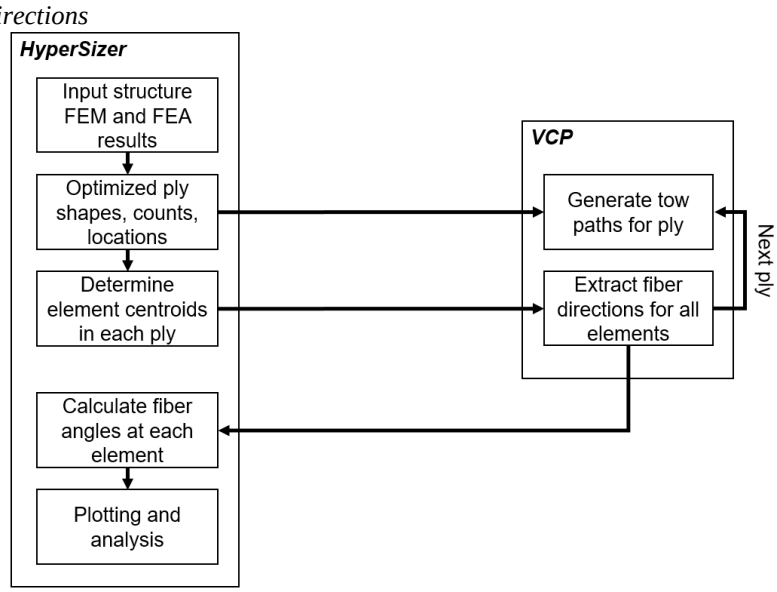

Figure 27. Flow diagram for updating HyperSizer with true fiber directions from VCP.

2. Mapping Laps and Gaps

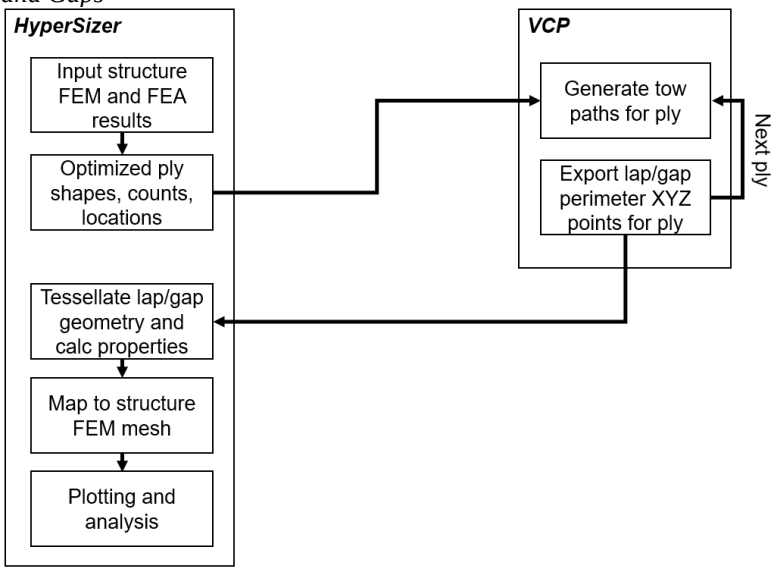

Figure 28. Flow diagram for updating HyperSizer with lap/gap data from VCP.

3. Mapping Steering Radius Violations

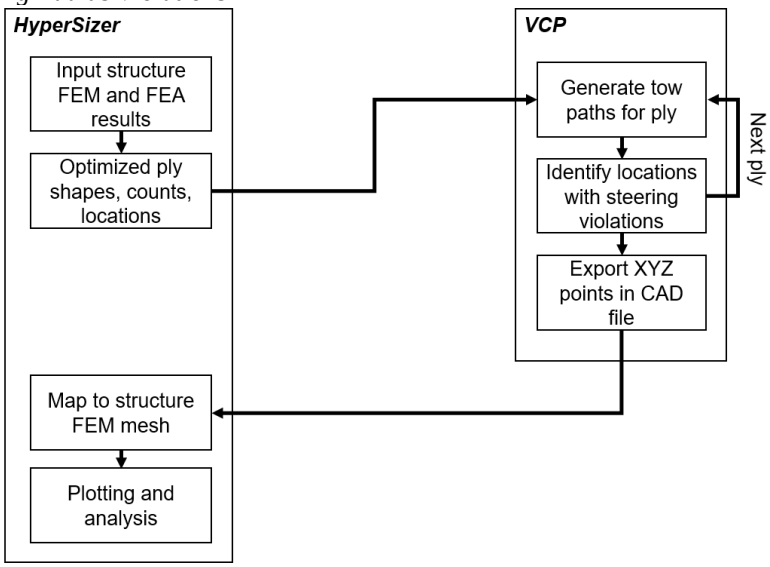

Figure 29. Flow diagram for updating HyperSizer with steering violation locations from VCP.

Acknowledgments

Thanks to Blaine Daronco and Phil Yarrington for software development and support. This work was performed under a contract task funded by NASA Langley Research Center as part of the Advanced Composites Project, Technical Challenge 3 of the NASA Advanced Aeronautical Vehicle Program.

References

[1] Stodieck, O., Cooper, J. E., Weaver, P. M., Optimisation of Tow-Steered Composite Wing Laminates for Aeroelastic Tailoring, *55th AIAA/ASME/ASCE/AHS/ASC Structures, Structural Dynamics, and Materials Conference*, National Harbor, Maryland, 2014

[2] Stanford, B. K., Jutte, C., V., Comparison of Curvilinear Stiffeners and Tow Steered Composites for Aeroelastic Tailoring of Transports, *34th AIAA Applied Aerodynamics Conference*, Washington, DC, 2016

[3] Groh, R. M., Weaver, P. M., Mass Optimisation of Variable Angle Tow, Variable Thickness Panels with Static Failure and Buckling Constraints, *56th AIAA/ASCE/AHS/ASC Structures, Structural Dynamics, and Materials Conference*, Kissimmee, FL, 2015

[4] Wu, K. C., et al, Design and Manufacturing of Tow-Steered Composite Shells Using Fiber Placement, *50th AIAA/ASME/ASCE/AHS/ASC Structures, Structural Dynamics, and Materials Conference*, Palm Springs, California, 2009

[5] HyperSizer, Software Package, Ver. 7.3, Collier Research Corporation, Newport News, VA, 2017.

[6] Vericut Composite Programming, Software Package, Ver. 7.4, CGTech, Irvine, CA, 2017.

[7] CATIA, Software Package, Ver. 5, Dassault Systems, Velizey, France, 2017.

[8] Tsai, S., & Hahn, H. (1980). *Introduction to Composite Materials*. Lancaster: Technomic Publishing Company.

[9] Tsai, S., & Wu, E. (1971). A General Theory of Strength for Anisotropic Materials. *Journal of Composite Materials*, 58-80.

[10] Croft, K., Lessard, L., Pasini, D., Hojjati, M., Chen, J., Yousefpour, A., "Experimental study of the effect of automated fiber placement induced defects on performance of composite laminates," *Composites Part A: Applied Science and Manufacturing*, Vol. 42, Issue 5., May 2011, p. 484-491.